Science of Sintering, **41** (2009) 175-184

doi: 10.2298/SOS0902175R

UDK 622.785:546.77:546.74

The Effect of Structural Changes during Sintering on the Electric and Magnetic Traits of the $Ni_{96.7}Mo_{3.3}$ Alloy Nanostructured Powder

L. Ribic-Zelenovic[1*)], M. Spasojevic[1], A. Maricic[1], M.M. Ristic[2]
[1]Joint Laboratory for Advanced Materials of SASA, Section for Amorphous Systems Technical Faculty, Čačak, Serbia
[2] Serbian Academy of Sciences and Arts, Belgrade, Serbia

Abstract:

$Ni_{96.7}Mo_{3.3}$ powder was electrochemically obtained. An X-ray diffraction analysis determined that the powder consisted of a 20% amorphous and 80% crystalline phase. The crystalline phase consisted of a nanocrystalline solid nickel and molybdenum solution with a face-centred cubic (FCC) lattice with a high density of chaotically distributed dislocations and high microstrain value. The scanning electronic microscopy (SEM) showed that two particle structures were formed: larger cauliflower-like particles and smaller dendrite-shaped ones. The thermal stability of the alloy was examined by differential scanning calorimetry (DSC) and by measuring the temperature dependence of the electrical resistivity and magnetic permeability. Structural powder relaxation was carried out in the temperature range of 450 K to 560 K causing considerable changes in the electrical resistivity and magnetic permeability. Upon structural relaxation, the magnetic permeability of the cooled alloy was about 80% higher than the magnetic permeability of the fresh powder. The crystallisation of the amorphous portion of the powder and crystalline grain increase occurred in the 630 K to 900 K temperature interval. Upon crystallisation of the amorphous phase and crystalline grain increase, the powder had about 50% lower magnetic permeability than the fresh powder and 3.6 times lower permeability than the powder where only structural relaxation took place.

Keywords: *NiMo powder, XRD, Magnetic permeability, Electric resistivity*

1. Introduction

Specific properties of amorphous and nanostructured metal alloys can be determined through their atomic and electronic structures.

Many AMAs (amorphous metal alloys) do not have simple or monocrystalline analogies, and their composition in the macrovolume could be changed within the single-phase state. This enables the homogenous alloys and the examination of the concentrational and temperature dependences of their properties.

The electronic structure determines a whole range of physical AMA properties (electroconductivity, TEMC, thermal conductivity, magnetic properties, optical conductivity

*) Corresponding author: lenka@tfc.kg.ac.rs

etc). With respect to that, a number of scientific papers [1-8] covering both theoretical and experimental topics have been published. However, certain properties of the electronic AMA structure have not been completely clarified. Particularly great difficulties exist when modelling the electronic structure of multiple component AMAs.

A great number of papers [8-20] presenting research results on the magnetic parameters of AMAs having different composition have been devoted to investigating AMA ferromagnetism. The interactions between d electrons of adjacent atoms are shown to be responsible for the ferromagnetism of the AMA on the basis of the iron group of metals, as well as in crystalline alloys. The concentrational disorder of atoms and different levels of defects play the leading role in the formation of magnetic properties.

The objective of this paper was to study the effect of structural changes during sintering on the electrical and magnetic properties of the electrochemically obtained powder of the $Ni_{96.7}Mo_{3.3}$ alloy.

Experimental

Electrochemical deposition of the $Ni_{96.7}Mo_{3.3}$ powder was performed in a glass 2 dm^3 electrochemical cell provided with a special compartment for a Lugin-capillary saturated calomel electrode. The anode was a 8 cm^2 platinum plate and the cathode was a 4.5 cm^2 titanium plate. The cell was located in a thermostat. The operating temperature was 298 ± 1K. The solution was prepared with p.a. chemicals (Merck) and triple-distilled water. The solution composition was: 0.035 mol dm^{-3} $NiSO_4 \cdot 7H_2O$; 0.007 mol dm^{-3} $Na_2MoO_4 \cdot 2H_2O$; 0.007 mol dm^{-3} NaCl and 07 mol dm^{-3} NH_4OH. The solution pH value was maintained in the 11 -11.5 range by adding ammonia solutions during the electrolysis. The $Ni_{96.7}Mo_{3.3}$ powder was obtained by galvanostatic deposition at a current density j=100 mA cm^{-2}. Upon electrolysis, the powder obtained was rinsed several times with triple-distilled water and then with 0.1% benzoic acid solution. Having been rinsed, the powder was dried at 360 K.

During electrochemical measurements, a standard electrical circuit composed of a programmer equipped with a potentiostat (RDE 3 POTENTIOSTAT Pine Instrument So. Grove City. Pennsylvania), digital voltmetres (Pro's Kit 03-9303C) and an electrochemical cell was used.

The chemical composition of the obtained powder was determined using a PEKTAR-A.A-200-VARIAN atomic absorber.

X-ray diffraction (XRD) was performed through a Diffractometer Philips PW 1710 with CuK_α (α = 0,154 nm) radiation and a graphite monochromator. XRD data were collected with a step mode of 0.03º with collection time of 1.5 s/step. Scanning electron microscopy (SEM) was conducted with a JEOL.JSM 5300 supplied with an EDS-QX·2000S spectrometer.

Differential scanning calorimetry (DSC) thermograms were obtained on a Shimadzu DSC-50 at a heating rate of 20 K min^{-1} under pure nitrogen flow.

Investigation of electrical properties was carried out using 40 x 1.2 x 0.5 mm samples, obtained by powder pressing under the pressure of 100 MPa. Electrical resistivity was measured by the four-point method within the temperature interval of 293 K to 950 K. The measurements were made in an argon atmosphere. Measurements of relative magnetic permeability were performed using the modified Faraday method, based on the action of an inhomogeneous field on the magnetic sample. The magnetic force measurements were performed with a sensitivity of 10^{-6} N in argon atmosphere.

Results and discussion

The nickel and molybdenum powder was obtained on a titanium cathode by electrochemical deposition from the solution 0.035 $NiSO_4 \cdot 7H_2O$ mol dm^{-3}, 0.007 $Na_2MoO_4 \cdot 2H_2O$ mol dm^{-3}, 0.007 NaCl mol dm^{-3} and 0.7 NH_3. mol dm^{-3} at a current density of 100 $mAcm^{-2}$.

The atomic absorption method determined that the chemical composition of the alloy was $Ni_{96.7}Mo_{3.3}$. The phase structure of the powder was determined using X-ray analysis. Based on the measured intensities and positions of the diffraction maximums and the JCPD standard, identification was made of the crystalline phases, as well as of the cell equation and microstructural parameters, including the mean crystallite dimension, microstrain and minimum density of the chaotically distributed dislocations. The Warren-Averbach method was used to determine the crystallite size distribution as well as the mean square root of the strain as a function of distance for the direction (111).

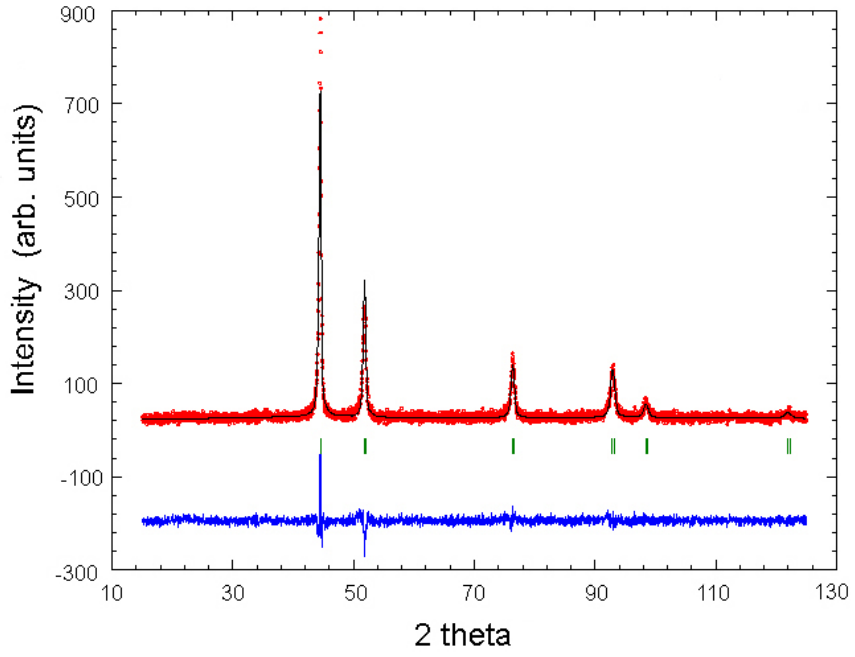

Fig. 1 Rietveld diagram of the initial $Ni_{96.7}Mo_{3.3}$ powder.

The dotted curve in Fig. 1 presents the measured values. The upper full line stands for the calculated values for the structural model. The bottom full line shows the difference between the measured and calculated values. The vertical lines (dashes) below the upper curves present positions of Bragg reflections for different FCC phase planes.

The X-ray in Fig. 1 shows that only one tesseral phase of the $Ni_{96.7}Mo_{3.3}$ solid solution was identified, the structure thereof being described in the Fm-3m space group. There were four well defined peaks in the diffractograph for different planes of the face-centred cubic FCC lattice of the $Ni_{96.7}Mo_{3.3}$ solid solution crystals. The cell equation parameters of the FCC phase were as follows: a=0.3254(2) nm, α=90º and V=0.043815(4) nm^3.
The microstructural data for the obtained FCC phase were as follows:

a) mean crystallite dimension value: 18.0 nm,
b) mean microstrain value: $1.9 \cdot 10^{-3}$
c) minimum density of the chaotically distributed dislocations: $8.7 \cdot 10^{11} cm^{-2}$.

The SEM records show that deposition at j=100 mAcm^{-2} resulted in the formation of two particle structures: larger cauliflower-like particles and smaller dendrite-shaped ones. The dendrites were formed on the surface of the cauliflower-like particles. Secondary and higher-order branches can be observed in the resulting dendrites (Figs. 2, 3 and 4).

A cauliflower particle where dendrite growth started (the dendrites appear as bright details) is presented in figure 2. Figure 3 shows a particle that started to grow as a dendrite, and then, during electrolysis, turned into a cauliflower at the top.

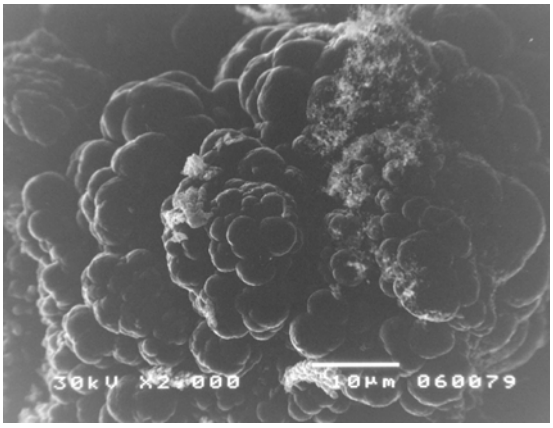

Fig. 2 SEM photograph of the $Ni_{96.7}Mo_{3.3}$ alloy powder

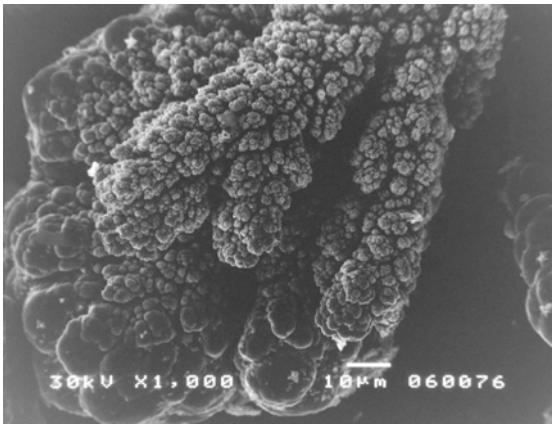

Fig. 3 SEM photograph of the $Ni_{96.7}Mo_{3.3.}$ alloy powder

Fig. 4 shows formed dendrites with secondary and higher-order branches.

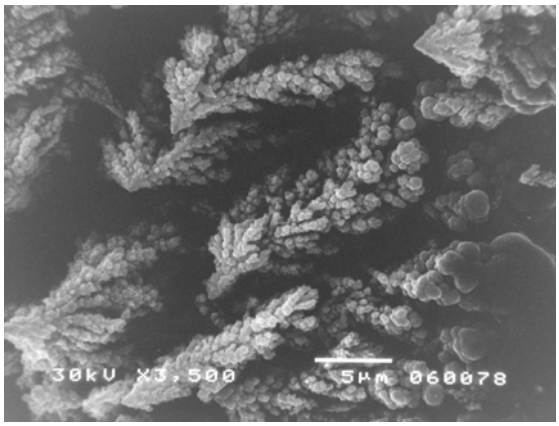

Fig. 4 SEM photograph of the $Ni_{96.7}Mo_{3.3}$ alloy powder

The thermal stability and structural changes during heating of the electrochemically obtained $Ni_{96.7}Mo_{3.3}$ powder at j=100 mAcm^{-2} were examined by differential scanning calorimetry (DSC) and by measuring electrical resistivity and magnetic permeability. The thermal stability was the function of the powder composition, crystal dimensions and dislocation densities. The thermogram in Fig. 5 shows two clearly pronounced maximums. The first sharp exothermal peak with a maximum at 650 K most likely resulted from crystallisation of the amorphous portion of the powder. The second peak, a considerably more pronounced and broader one, with a maximum at 770 K, was due to the growth of larger

crystals at the expense of smaller ones and structure rearrangement due to dislocation density and microstrain decreases (Figs. 5, 7 and 8).

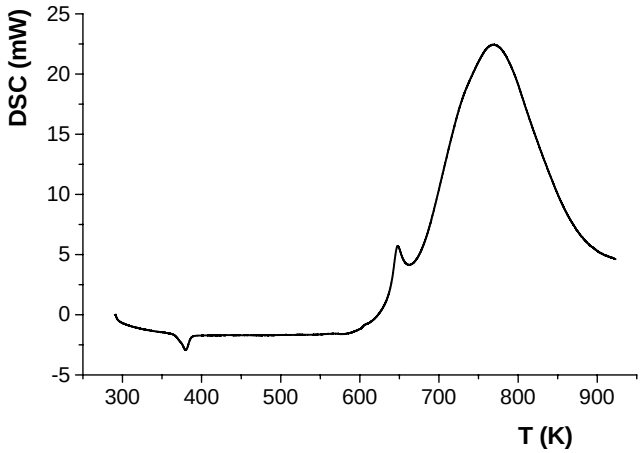

Fig. 5 DSC thermogram of the $Ni_{96.7}Mo_{3.3}$ alloy powder. The heating rate was 10ºC $min^{-1.}$

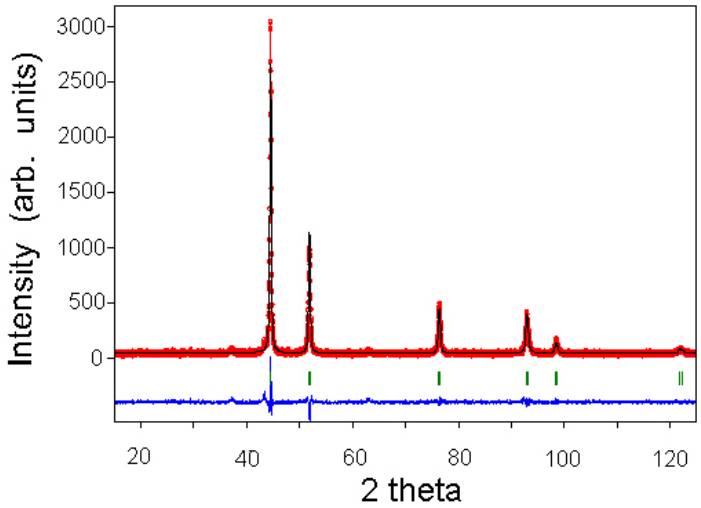

Fig. 6 Rietveld diagram of the $Ni_{96.7}Mo_{3.3}$ powder annealed for 30 min at 900 K in an argon environment.

The thermogram in Fig. 5 shows that no crystallisation of the amorphous portion of the powder was observed at temperatures up to 600 K. The thermal stability of the powder was also examined by X-ray analysis. The $Ni_{96.7}Mo_{3.3}$ powders were annealed at 900 K for a certain period of time. Subsequently, they were cooled to 298 K and X-rays were recorded (Fig. 6). The same FCC phase peaks always appeared in the obtained X-rays of the powders annealed for different lengths of time. The peaks of the annealed powders were considerably narrower and had a four times higher intensity. A detailed Rietveld analysis of diagrams obtained for the fresh and annealed powders suggested that during annealing at 900 K the following occurred:

a) complete transformation of the amorphous portion of the powder into a crystalline one,
b) an increase in the crystal grain size,
c) a decrease in the minimum density of the chaotically distributed dislocations and
d) a decrease in the mean microstrain (Figs. 6, 7 and 8).

The crystal grain size depended on the annealing duration. The increase in annealing time led to the formation of larger crystalline grains having fewer dislocations. Fig. 7 shows that the crystallite dimensions of the initial powder (curve a) were smaller than those of the annealed powder (curve b).

Fig. 8 presents the distance dependence of the mean square root of the strain for the fresh powder (a) and the powder annealed at 900 K(b). The powder annealing resulted in a considerable decrease in the mean square root of the strain.

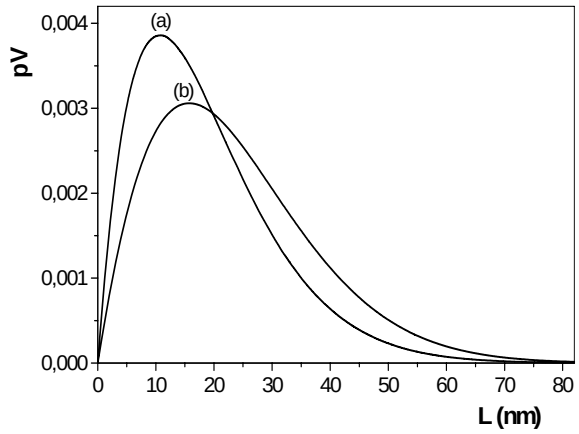

Fig. 7 Crystallite size distribution for the $Ni_{96.7}Mo_{3.3}$ powder: a) non-annealed powder and b) powder annealed for 30 min at 900 K in an argon atmosphere.

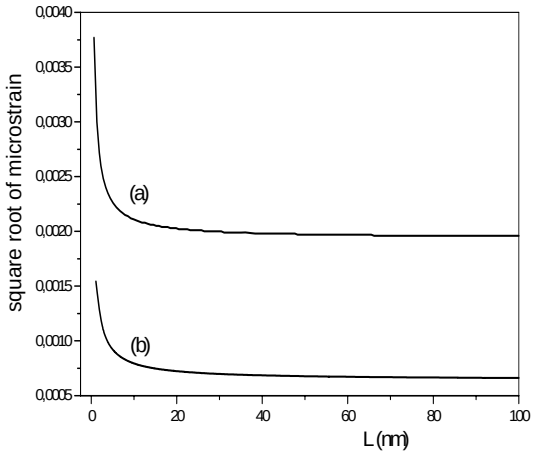

Fig. 8 Distance-dependent mean square root of the strain for the $Ni_{96.7}Mo_{3.3}$ powder: a) non-annealed powder and b) powder annealed for 30 min at 900 K in an argon atmosphere.

Structural changes of the $Ni_{96.7}Mo_{3.3}$ powder were observed by measuring the dependence of the electrical resistivity on the heating temperature. Fig. 9 shows a thermogram (curve a) and the temperature dependence of the electrical resistivity (curve b).

As seen from Fig. 9, during annealing of the $Ni_{96.7}Mo_{3.3}$ powder obtained at j=100 $mAcm^{-2}$, the resistivity increased linearly with increasing temperature over the interval of 300 K to 450 K, indicating that structural changes in the powder did not take place in the above temperature interval. The line slope was a complex function of the crystal grain size, the proportion of the amorphous phase, the number of microstrain dislocations and the molybdenum content. The more irregular the pressed powder structure, i.e. the higher the dislocation number and the higher the amorphous phase proportion, the lower the electron

number in the conduction zone, and hence the temperature increase led to the transfer of a number of localised electrons from the defective places into the conduction zone, causing a low slope. In the 450 K to 560 K temperature interval, the resistance decreased with increasing temperature. The thermogram (curve a) shows that there were no significant changes in the temperature interval, indicating that structural relaxation occurred in the $Ni_{96.7}Mo_{3.3}$ pressed powder within the above-stated temperature range. The radiograph recorded after the 60-minute powder annealing at 570 K did not differ significantly from the fresh powder radiograph, which confirmed that it was only structural relaxation and not crystallisation that took place at temperatures up to T=570 K. The high drop in resistivity within the temperature interval of the structural relaxation resulted from free volume and microstrain decreases, which induced an increase in electron numbers in the conduction zone. The resistivity drop was also due to better contact established between the powder particles.

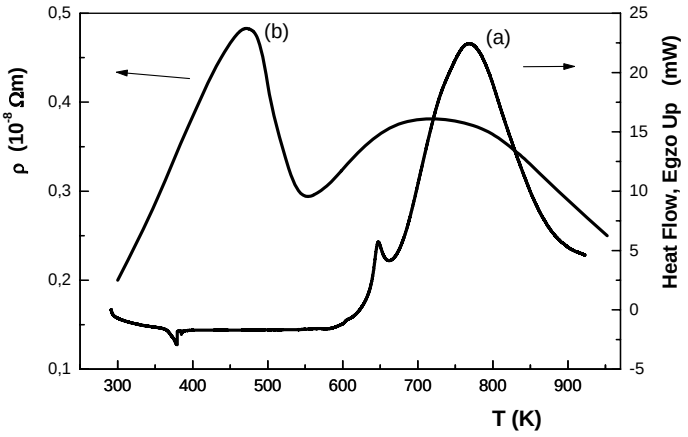

Fig. 9 DSC thermogram (curve a) and temperature dependence of the electrical resistivity (curve b) of the $Ni_{96.7}Mo_{3.3}$ alloy. Heating rate 10 K min^{-1}.

In the temperature interval of 560 K to 630 K, the resistivity linearly increased again, indicating the absence of significant structural changes in the interval. The $Ni_{96.7}Mo_{3.3}$ alloy was annealed for 60 minutes at 630 K and then cooled down to room temperature and the resistivity was simultaneously measured. The electrical resistivity reduced linearly with decreasing temperature. The pressed powder was heated again to 630 K. An identical linear dependence of the electrical resistivity on temperature was observed during the repeated heating, a line being obtained during the cooling process. This indicated that the structural relaxation process terminated after 60 minutes of sample heating at 630 K. The slope of the above linear dependence was higher than that of the linear dependence of resistivity on the fresh powder temperature in the temperature interval 300-450 K. The reduction in the rate of the increase of resistivity in the temperature interval 630-700 K resulted from a) crystallisation of the amorphous portion of the powder, b) crystal grain growth, c) decrease in dislocation density and from d) termination of the electron-magnon interaction at temperatures higher than the Curie temperature (660 K). At temperatures higher than 700 K resistivity decreased due to the crystal grain increase and dislocation density decrease. The $Ni_{96.7}Mo_{3.3}$ pressed powder was isothermally annealed for 30 minutes at 900 K. Upon annealing, the sample was cooled at a rate of 10 K min^{-1} to room temperature and electrical resistivity was simultaneously measured. Electrical resistivity linearly decreased. The line slope was higher than the one obtained during the first annealing of the powder and the second one obtained during the fresh sample heating within the temperature range of 560 K to 630 K and 300 K to 450 K, respectively.

The obtained results on the measurement of the temperature dependence of electrical resistivity were correlated with the X-ray and DSC results.

The magnetic properties of the electrochemically obtained $Ni_{96.7}Mo_{3/3}$ were also dependent on the molybdenum content, the proportion of crystalline and amorphouse phases, the crystal grain size, the dislocation density and the microstrain. Figure 10 presents the temperature dependence of the relative magnetic susceptibility of the $Ni_{96.7}Mo_{3.3}$ pressed powder. It shows that the relative magnetic permeability of the pressed powder did not change significantly with increasing temperature in the temperature interval of 300 K to 450 K since structural changes did not occur within this temperature interval. In the temperature interval 450 K to 560 K relative magnetic permeability increased with increasing temperature, reaching its maximum at about 560 K. The increase in relative magnetic susceptibility resulted from structural relaxation during which partial thermal stabilisation of the pressed powder occurred, i.e. the free volume and internal microstrains decreased, and the regularity of the structure at a short distance increased. This induced a decrease in the interatomic distances and better overlap of the d-orbitals of adjoining atoms, and, hence, an increase in the interaction integral and, therefore, increases in the mutual interaction energy and magnetic permeability. This all provided better mobility of the magnetic domain walls and their better orientation, and hence higher magnetic permeability.

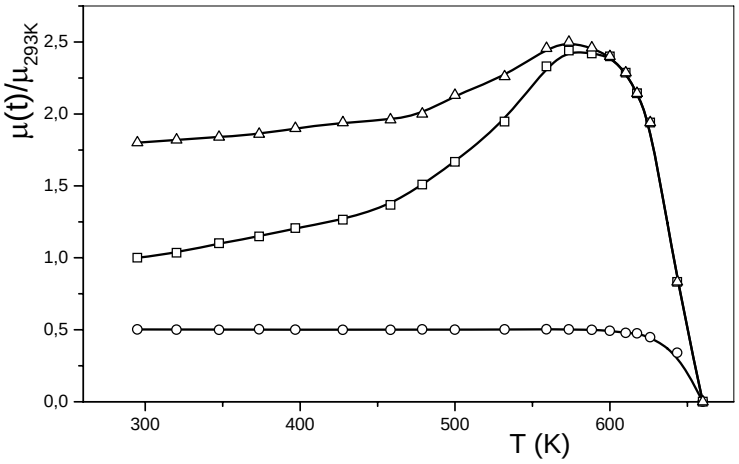

Fig. 10 Temperature dependence of the relative magnetic permeability of the pressed powder of the $Ni_{96,7}Mo_{3,3}$ alloy: □ – first heating, Δ - second heating, ○ – third heating. Heating rate of 20 K min^{-1}.

During heating of the alloy at 560 K to 660 K, the relative magnetic permeability decreased gradually at first and, then, rapidly at higher temperatures, reaching the zero value at the Curie temperature of 660 K. At temperatures higher than 560 K, the thermal motion energy became sufficiently high to be able to exceed the interaction energy between adjoining atoms providing spin parallelism. Following the first heating, the alloy was cooled to room temperature and then reheated to the Curie temperature. During the second heating, the relative magnetic susceptibility did not change in the temperature interval of 300 K to 560 K, and its value was equivalent to the maximum obtained during the first heating, which proved that the thermal stabilisation (structural relaxation) process completely terminated during the first heating.

The $Ni_{96,7}Mo_{3,3}$ alloy was then annealed for 30 minutes at 900 K for complete crystallisation of the amorphous portion of the powder and for crystal grain increases and substantial dislocation annihilation. Upon annealing, the alloy was cooled to room temperature and then reheated gradually up to the Curie point.

During the third heating, within the temperature interval of 300 K to 560 K, the magnetic permeability did not change, its value being about 50% lower than that of the fresh powder.

Conclusion

The X-ray analysis determined that the $Ni_{96.7}Mo_{3.3}$ alloy powder electrochemically obtained at a current density of 100 mA cm^{-2} comprised 20% amorphous phase and 80% nanocrystalline phase. During sintering of this powder, irretrievable structural changes occurred affecting the electrical and magnetic properties. The crystallite size of the non-annealed powder was lower than that of the powder annealed at 900 K. Powder annealing resulted in a considerable reduction of the mean microstrain value.

Measurements of the electrical resistivity and magnetic permeability during heating showed that structural relaxation took place within the temperature interval of 450 K to 560 K. During the process, fine interatomic shifts occurred causing free volume and microstrain decreases in the alloy, as well as a simultaneous decrease in interatomic distances and an increase in distance regularities providing better overlaps of the d orbitals of adjoining atoms and increased exchange interaction. These changes caused higher mobility of the magnetic domain walls and their better orientation. All these processes resulted in an increase in magnetic permeability.

Following the structural relaxation, the magnetic permeability of the cooled alloy was found to be about 80 % higher than that of the fresh powder. Upon crystallisation of the amorphous phase and following the crystal grain increase, the magnetic permeability of the cooled samples was about 50 % and 3.6 times lower than that of the fresh and relaxed powders, respectively.

Acknowledgements

This study was supported by the Ministry of Science and Technology of the Republic of Serbia (Project 142011G) and Projects F/7 and F/198 supported by the Serbian Academy of Sciences and Arts.

References

1. L.V.Panina, K.Mohri, J.Magn. Soc.Jpn. 19 (1995) 265.
2. Y.K. Kim, W.S. Cho, T.K.Kim, C.O.Kim, H.B.Lee, J. Appl. Phys. 83(1998) 6575.
3. U. Köster, U.Herald, Crystallization of Metallic Glasses, Springer, New York, 1981, pp. 225-259.
4. B.Z.Jiang, A.N.Ulyanov, S.C.Yu, H.B.Lee, S.T.Park, J.Appl.Phys. 91 (2002) 8444
5. M.V.Šušić,Y.M.Litvinenko, Z.Metall. 79 (1988) 20.
6. D.M.Minić, A.M.Maričić, R.Ž.Dimitrijević; M.M.Ristić, J. Alloys Compnd. 430 (2007) 241.
7. A.M.Maričić, D.M. Minić, T.Zak, Sci.Sinter. 36 (2004) 197.
8. S. S. Jaswol Phys. Rev.B: Condens. Matter 34 (1986) 8937.
9. W.Y. Ching, G. Zhao, Y. He Phys. Rev. B, 42 (1990) 10878.
10. L.Ribić-Zelenović, L.Rafailović, M.Spasojević, A.Maričić, Sci. Sintering, 38 (2006) 145.
11. S.N.Kaul, W.Kettler and M.Rosenberg, Phys.Rev.B 33 (1986) 4987.
12. Y. Kakehashi, Mater. Sci. Eng. A, 179 (1994) 62.

13. L.F.Barquin, J.R.Hernandez, J.J.Gomez Sal, J. Magn. Magn. Mater. 83 (1990) 357.
14. J.S.Song, H.B.Im, M.S.Yun, J.Appl. Phys. 69 (1991) 5014
15. M.Spasojević, A.Maričić, L.Rafailović, Sci. Sintering, 36 (2004) 105.
16. A.Kalezić-Glišović, N.Mitrović, A.Maričić, R.Simeunović, Mat.Sci. Forum, 555 (2007) 533.
17. L.Ribić-Zelenović, R. Simeunović, A.Maričić, M.Spasojević, Mat.Sci. Forum 555 (2007) 539.
18. L.Ribić-Zelenović, L.Rafailović, A.Maričić, M.Spasojević, J. Optoelectron. Adv.Mater., 9 (2007) 2681.
19. L. Ribić-Zelenović, L. Rafailović, M. Spasojević, A. Maričić, Physica B, 403 (2008) 2148.
20. L.Ribić-Zelenović, M.Spasojević, A.Maričić, M.Ristić, J. Optoelectron. Adv. Mater., 10 (2008) 1384.

Садржај: *Електрохемијским поступком добијен је прах $Ni_{96,7}Mo_{3,3}$. Рендгенском анализом (XRD) је установљено да се прах састоји од 20% аморфне и 80% кристалне фазе. Кристалну фазу чини нанокристални чврсти раствор никла и молибдена са површински центрираном кубном решетком (FCC) са великом густином хаотично распоређених дислокација и великом вредношћу микронапрезања. Скенирајућом електронском микроскопијом (SEM) показано је да настају два облика честица: крупније честице облика карфиола и ситније честице облика дендрита. Термичка стабилност легуре испитивана је диференцијалном скенирајућом калориметријом (DSC) и мерењем зависности електричне отпорности и магнетне пермеабилности од температуре. Структурна релаксација праха одвија се у температурској области од 450 K до 560 K узрокујући знатне промене електричне отпорности и магнетне пермеабилности. Након структурне релаксације, магнетна пермеабилност охлађене легуре већа је за око 80% од магнетне пермеабилности свежег праха. Кристализација аморфног дела праха и пораст кристалних зрна одвија се у температурској области од 630 K до 900 K. Прах након кристализације аморфне фазе и пораста кристалних зрна има мању магнетну пермеабилност од свежег праха за око 50% и 3,6 пута мању пермеабилност од праха у коме се одвила само структурна релаксација.*

Кључне речи: *Прах NiMo, рентгенска дифракција, магнетна пермеабилност, електрична отпорност.*